Journal of Saudi Chemical Society (2020) **24**, 267–281

King Saud University

**Journal of Saudi Chemical Society**

www.ksu.edu.sa
www.sciencedirect.com

ORIGINAL ARTICLE

# Remediation of azo-dyes based toxicity by agro-waste cotton boll peels mediated palladium nanoparticles

**Boya Palajonnala Narasaiah, Badal Kumar Mandal** *

*Trace Elements Speciation Research Laboratory, Department of Chemistry, School of Advanced Sciences, Vellore Institute of Technology (VIT), Vellore-14, Tamil Nadu, India*

Received 10 July 2019; revised 3 November 2019; accepted 23 November 2019
Available online 10 December 2019

**KEYWORDS**

Cotton boll peels;
Pd NPs;
Azo-dyes;
Nano-catalyst;
Industrial effluents;
Wastewater

**Abstract** The present study reports an environmental benign route for the synthesis of palladium nanoparticles (Pd NPs) using agro-waste empty cotton boll peels aqueous extract for the first time. Surface Plasmon Resonance (SPR) band in absorption spectrum of Pd NPs at 275 nm confirmed the formation of Pd NPs by using UV–Vis spectroscopy. Crystalline nature of Pd NPs was confirmed by powder XRD analysis. Size and morphology was studied by transmission electron microscopy (TEM). The cotton peels extract acted as a source of phytochemicals which primarily reduced $Pd^{+2}$ to $Pd^{0}$ nanoparticles (Pd NPs) and imparted stability of Pd NPs by surface capping. The characteristic functional groups of phytochemicals in extract and capped Pd NPs surfaces were identified by FT-IR analysis. Catalytic activity of the synthesised Pd NPs was checked against reduction of hazardous azo-dyes such as Congo red, Methyl orange, Sunset yellow and Tartrazine with $NaBH_4$ as electron donors. Pd NPs catalysed reduction of all azo-dyes by $NaBH_4$ in aqueous medium was monitored by UV–visible spectroscopy where Pd NPs mediated transfer of electrons from $NaBH_4$ to azo-dyes as carrier. The synthesized Pd NPs acted as a good catalyst and could be a promising material in degrading toxic azo-dyes from industrial effluents and wastewater.


## 1. Introduction

Nanoparticles with high surface area to volume ratio show enhanced physical and chemical properties and find different applications in electronics, catalysis, antimicrobial and antioxidant activity, and industrial wastewater treatment [1–3]. Among metal NPs Pd NPs have huge applications in nanotechnology because of their good catalytic activity, electrical conductivity, chemical stability and biological activity [4,5]. The properties of NPs depend mainly on their size, shape,

* Corresponding author.
E-mail address: badalmandal@vit.ac.in (B.K. Mandal).
Peer review under responsibility of King Saud University.

ELSEVIER Production and hosting by Elsevier

https://doi.org/10.1016/j.jscs.2019.11.003
1319-6103 

structure, morphology and chemical composition [6–8] which promoted researchers to synthesise tiny NPs employing physical, chemical and biological methods [9,10]. Normally physical and chemical methods are expensive and require high temperature, pressure and energy. In the chemical synthetic route the starting materials, reactants and solvents used are toxic and potentially hazardous to environment. Hence there is a continuous demand in developing benign synthetic routes for the syntheses of NPs without using toxic/hazardous chemicals and solvents [11]. Nowadays several methods are available for the synthesis of nanomaterials, but among them green methods are getting more importance due to several advantageous such as reduction in uses of toxic and hazardous chemicals [12]. Synthesis of metal and metal oxide NPs by using plant extract has worked so well because it behaved as both reducing agent and capping agents [13]. Plants have different phytochemical constituents i.e. secondary metabolites such as flavonoids, terpenoids, alkaloids, antioxidants and sugars in leaves, seeds, fruits peels a well as others parts of the plants which can be used for synthesis of nanomaterials replacing the potential hazardous chemicals [14]. Green synthesis of nanomaterials using plant extracts has been suggested as the alternative to physical and chemical methods due to their non-toxic nature and cheap [15]. There are many reports available for the synthesis of Pd NPs using different plants extracts [16–18]. Among different nanomaterials, Pd NPs has gained the great interest in heterogeneous and homogeneous catalysis field as well as in biological applications [19–22].

Also, different articles have reported the size-controlled synthesis of metal NPs by tuning surface area to volume ratio, concentration of the reactants, quantities of extract, process temperature and pH of the solution, etc [23–25]. Mostly metal and metal oxide NPs, metal supported such as metal/non-metal doped $CeO_2$ NPs [28], L-arginine-functionalized $Fe_3O_4$ NPs [29], titanium dioxide supported silver NPs [30], Ag/zeolite nanocomposite [31], Pt NPs [32] and Pd NPs [33] have been synthesized using green method for the degradation of dyes [34].

Water pollution is one of the major environmental issues due to reckless human and uncontrolled industrial activities resulting emission of large amount of dyes from textile industry, paper industry and tanneries. Water pollution causes serious effect to aquatic environment and human life. The water soluble dyes are non-degradable and pollute all types of water. Thus the removal of dyes such a Sunset Yellow, Methyl Orange (MO), Tartrazine and Congo red plays a major role in wastewater treatment, because azo-dyes are highly carcinogenic and mutagenic in nature. Earlier researchers used different techniques for degradation of dyes such as Fenton oxidation for MO degradation [26]. Gholami-Borujeni et al. [20] reported Acid Orange 7 dye decolorization from textile wastewater by using enzyme and $H_2O_2$ treatment. Rostami-Vartooni et al. [27] used perlite supported Ag NPs for the reduction of 4-nitrophenol and Congo red.

The present study focused on the biosynthesis of Pd NPs using agro-waste empty cotton boll peels (ECBP) aqueous extract for the first time. The synthesized Pd NPs was characterized by different instrumental techniques. Finally the synthesized Pd NPs was used as an efficient green catalyst for the reduction of organic pollutant dyes such as Sunset yellow, Methyl orange, Tartrazine and Congo red by $NaBH_4$ as electron donors at room temperature. The catalytic reduction was monitored and a possible mechanism of azo-dyes reduction is proposed.

## 2. Material and methods

### 2.1. Materials

Palladium chloride ($PdCl_2$), Congo red (CR), Tartrazine (TZ), Methyl orange (MO), Sunset yellow (SY) and other highly pure chemicals were purchased from Sigma Aldrich, India while ECBPs (Fig. S1A) were collected from the cotton crop at Chilakaladona, Mantralayam, Kurnool of Andhra Pradesh, India.

### 2.2. Extract preparation

The ECBP was washed with pure water and was cut into small pieces and dried followed by repeated washing with hot water to remove any soluble matter followed by drying overnight at room temperature. The dried ECBP was grinded and sieved by 100 mesh sieving net. Then 3 g ECBP powder was added to 100 mL distilled water and heated on water bath at 80 °C for 50 min to prepare aqueous extract. The extract was cooled to room temperature and filtered through Whatman filter paper No.1. Then the freshly prepared extract was used for the synthesis of Pd NPs (Fig. S1B).

### 2.3. Synthesis of Pd NPs and purification

Pd NPs was prepared by the addition of 30 mL plant extract to 15 mL palladium chloride solution (5 mM) by stirring using a magnetic stirrer for 2 h at 60 °C and then UV–Vis spectroscopic study was carried out to confirm the formation of Pd NPs. Also, the brown colour colloidal solution of Pd NPs confirmed its formation. Then the colloidal solution of Pd NPs was centrifuged at 4000 rpm for 30 min, filtered, dried and the residue/pellet was dispersed in ethanol twice and washed thrice with double distilled water to remove impurities and unused chemicals. Finally the residue was dispersed in 2 mL double distilled water, filtered, dried and used for further characterization techniques.

### 2.4. Determination of total phenolic compounds

Total phenolic content in ECBP aqueous extract was determined by using Folin-Ciocalteu (FC) reagent with the help of spectrophotometer [35]. In briefly, 1 mL extract was mixed with 2 mL FC reagent (10%) and then 4 mL sodium carbonate solution (5%) was added. The reaction mixture was incubated at 37 °C for 30 min in an incubator and the resulting deep blue colour solution showed an absorbance peak at 756 nm by UV–Vis spectrophotometry. Standard gallic acid was used as reference for phenolic content. ECBP aqueous extract contained total phenol content of 296 mg/g. A plausible mechanism of Pd NPs synthesis is presented in Fig. S1B.

### 2.5. Characterization of Pd NPs

Initially the formation of Pd NPs was characterized by using UV–visible spectrophotometer (V-670 Jasco). The synthesized

colloidal solution was centrifuged at 4000 rpm and washed with double distilled water several times. Finally the pellet was dispersed in ethanol, centrifuged and dried for the further characterisation. The Fourier Transform Infrared (FT-IR) spectra were recorded using affinity-1 FT-IR (Japan, Shimadzu instrument) in the region of 500–4000 $cm^{-1}$ with a resolution of 4 $cm^{-1}$ by KBr disc method. The crystallinity and size of Pd NPs powder was characterized by using powder X-ray diffraction (Bruker D8 advanced diffractometer) with Cu Kα radiation (λ = 1.54 Å) in 2θ range from 10° to 90° at a scanning rate of 4°/min and step-size increase of 0.02°. XRD analysis was carried out after calibrating instrument with lanthanum hexaboride as a reference material. The size, shape i.e. morphology and selected area electron diffraction (SAED) pattern were determined by HR-TEM (JEOL JEM 2100) which was operated with an acceleration voltage of 200 kV with a resolution of 0.1 nm. For microscopic analysis Pd NPs was well dispersed in water by ultrasonication and then few drops of sample was placed on carbon coated Cu grid and dried before analysis.

### 2.6. Catalytic reduction of azo-dyes

In the present study catalytic activity of Pd NPs was checked against reduction of azo-dyes such as Sunset yellow, Methyl orange, Tartrazine and Congo red by $NaBH_4$ as electron donor. In brief, 3 mL each dye solution ($1 \times 10^{-4}$ M) was mixed with 150 µL (0.05 M) freshly prepared $NaBH_4$ and then 60 µL of Pd NPs colloidal solution (1 µg/µL) was added. Finally reduction of dyes was monitored with time by UV–Visible spectroscopy after measuring absorbance of dye solution at 425.8 nm for Tartrazine, 462.8 nm for Methyl orange, 483.4 nm for Sunset yellow and 496.2 nm for Congo red. Under similar conditions reduction of dye was monitored by varying amount of Pd NPs (80 µg, 100 µg and 120 µg) or concentration of Congo red dye solution ($0.4 \times 10^{-4}$ M, $0.6 \times 10^{-4}$ M and $0.8 \times 10^{-4}$ M) by UV–Visible spectroscopy.

## 3. Result and discussion

Formation of Pd NPs was confirmed by UV–Visible spectroscopy (Fig. 1). UV–Vis spectroscopy analysis of empty cotton boll peels extract showed two absorption bands at around 248 nm and 255 nm which appeared due to π → π* transitions of electrons in polyphenols present in the extract (Fig. 1A) [36]. The reduction of $Pd^{+2}$ to $Pd^0$ NPs was monitored by checking surface Plasmon resonance (SPR) band at 275 nm using UV–Visible spectrophotometer. The single absorption band at 275 nm suggested the formation of spherical shaped Pd NPs (Fig. 1B) [37].

The XRD analysis was carried out within 2θ values of 10–90° to check crystalline nature and correct phase formation of Pd NPs. Fig. 1C demonstrates the XRD pattern of the synthesized Pd NPs and XRD pattern displays characteristic reflection planes with hkl values of 111, 200, 220 and 311 at 2θ values of 39.71°, 46.36°, 67.66° and 81.42°. The clear sharp peak at Bragg angle 2θ of 39.71 reflects the plane (1 1 1) of face centred cubic crystal structure of Pd NPs. Mostly Pd NPs was oriented along the (1 1 1) plane with intense peak and the enlargement of the Bragg's peaks indicates the formation of crystalline NPs. The XRD pattern of the synthesized Pd NPs supported to the reference XRD pattern for standard Pd NPs reported by joint committee on powder diffraction standard with data card no as JCPDS N0: 41-14-45. The average crystallite size was calculated by using Scherrer's equation as

$$D = 0.89\lambda/\beta\mathrm{Cos}\ (\theta)$$

where, $D$ is the average crystallite size, $\beta$ is the (1 1 1) plane of full-width at half maximum (FWHM) intensity, $\lambda$ is the X-ray wavelength of radiation (1.54 Å), $\theta$ is Bragg's angle ($2\theta$). The average crystallite size was calculated as 9.44 nm.

The stability of synthesized Pd NPs (pH 6.93) was analysed by dynamic light scattering (DLS) study. Normally zeta potential value higher than ±28.00 eV suggests good stability of any particles dispersion i.e. colloidal solution. In addition, polydispersity index (PDI) value having less than 0.5 indicates high colloidal stability or minimum sedimentation potential. Fig. 1D show the zeta potential value of Pd NPs aqueous dispersion as −62.5 mV and the higher zeta potential value suggests higher electric charge on the surface of the particles which leads to higher electrostatic repulsion between the colloidal NPs due to more electrophoretic mobility i.e. minimizing nucleation and aggregation/sedimentation. The obtained result shows excellent stability of Pd NPs which is similar to other published report [38]. DLS technique is used to look into the size distribution of Pd NPs aqueous dispersion (Fig. S2). It displays an average particle size of 268.4 nm and the particles show good dispersion with a polydispersity index of 0.447 suggesting high colloidal stability. The synthesized Pd NPs is dispersed both in acidic medium (pH 2.32) and basic medium (pH 9.24) and DLS analysis of them shows particles size distribution (Fig. S3). The zeta potential value of Pd NPs aqueous dispersion in acidic medium (pH 2.32) is −28.7 mV with an average particle size of 625.0 nm and PDI of 0.493, whereas in basic medium (pH 9.24) its zeta potential is −42.2 mV with an average particle size of 308.8 nm and PDI of 0.473 (Fig. S3). These results clearly suggest that Pd NPs aqueous dispersion is sufficiently stable both in neutral and basic solutions. A similar range of Pd NPs size distribution (322 nm) was reported by Hazarika et al. [39] where Pd NPs was synthesized using aqueous leaf extract of *Garciniapedunculata* Roxb.

Normally phytochemicals present in peels extract act as reducing and stabilizing agent during the synthesis of Pd NPs from its salt. The capping of phytochemicals on the surface of Pd NPs was checked by identifying the functional groups attached to Pd NPs surfaces using FTIR analysis. FTIR analysis was carried out for the residue of the peels aqueous extract after solvent evaporation and synthesised Pd NPs. Fig. 2A shows the FTIR-spectrum for the residue of ECBP aqueous extract after solvent evaporation and the strong absorbance peak at 3369.64 $cm^{-1}$ corresponds to —OH group stretching vibration of polyols, peak at 2904.80 $cm^{-1}$ for aromatic ring —C—H stretching vibration, peak at 2114.16 $cm^{-1}$ for —C≡C— stretching vibration, peak at 1620.21 $cm^{-1}$ for aromatic ring —C=C— stretching vibration, weak peak at 1332.81 $cm^{-1}$ for —O—H bending vibration, and peak at 1247.94 $cm^{-1}$ for —C—O stretching vibration respectively. In addition, the weak bands at 1074.35 $cm^{-1}$ and 941.26 $cm^{-1}$ correspond to —C—O—C— and —N—H bending vibration respectively. The above mentioned bands appeared due to the presence of polyphenols such as flavonoids, alkaloids and phenolic acids, terpenoids and proteins compounds which are abundantly present in ECBP

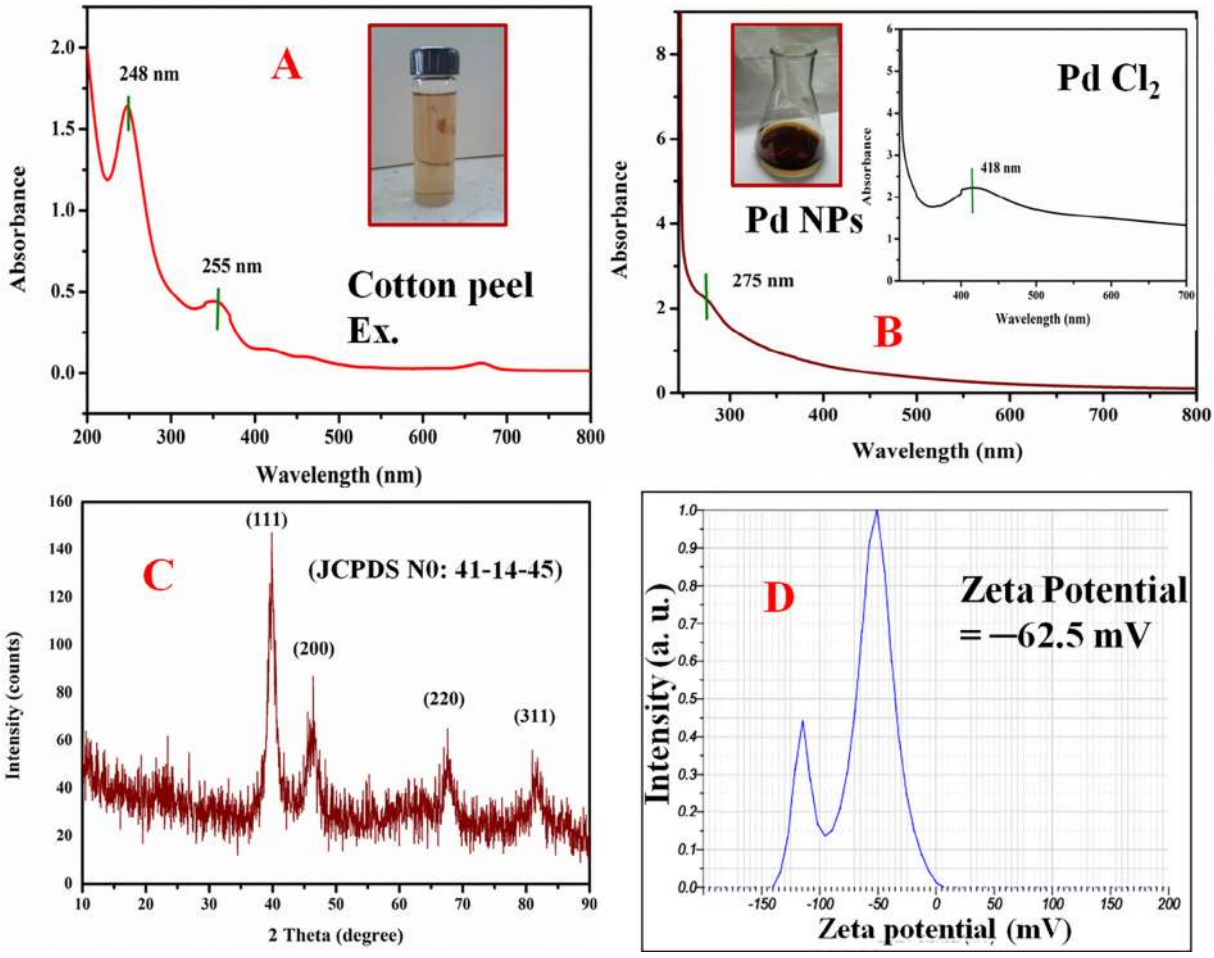


**Fig. 1** UV–Vis spectra of cotton peels extracts (A), synthesized Pd NPs using aqueous cotton peels extracts (inset UV–Vis spectrum of Pd chloride solution (B), XRD pattern of synthesized Pd NPs (C) and zeta potential of Pd NPs aqueous dispersion by DLS analysis (D).

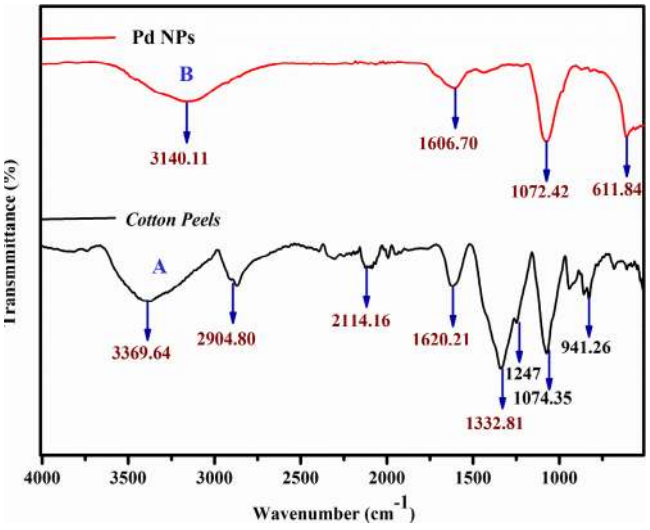


**Fig. 2** FT-IR spectra of cotton peels (A) and synthesized Pd NPs using cotton peels aqueous extracts (B).

aqueous extract and responsible for the bioreduction and stabilization of Pd NPs [40,41].

After reduction of Pd-salts to Pd NPs some minor changes in peaks position and intensity were observed in FTIR spectrum (Fig. 2B) which suggest the participation of phytochemicals such as polyphenols, phenols, flavonoids, proteins and alkaloids with functional groups i.e. carboxylic acid, ketones, amines and alcohol in the bio-reduction [42]. The significant narrow peak at 3369 $cm^{-1}$ could be assigned to —OH group of polyphenolic compounds. Some peaks of Pd NPs in FTIR spectrum were shifted slightly i.e. peaks at 3369, 1620, 1074 $cm^{-1}$ were shifted to 3140, 1606.7, 1072.4 $cm^{-1}$, whereas a new stretching vibration peak appeared at 611.8 $cm^{-1}$ and peaks at 2904.8, 2114.16, 1332.8, 1247, 941 $cm^{-1}$ disappeared in FTIR spectrum of Pd NPs (Fig. 3B). These results suggest that original polyphenolic phytochemicals were transformed to the respective ketone forms which provided stability to Pd NPs [25].

The phyto-constituents in aqueous extract of ECBP were screened by HPLC analysis (Perkin Elmer 200 Series HPLC) equipped with UV–Vis detector and 200 Series pump. The mobile phase consisted of 0.1 M KCl and 32% acetonitrile whose pH was 3 adjusted by using dil. HCl. The compounds were separated by Brownlee Analytical C-18 (150*4.6 mm, 5 μm, 110 Å) column and it was packed with 5 μm silica particles with a $\lambda_{max}$ 275 nm. The flow rate was 1 mL $min^{-1}$. Gen-

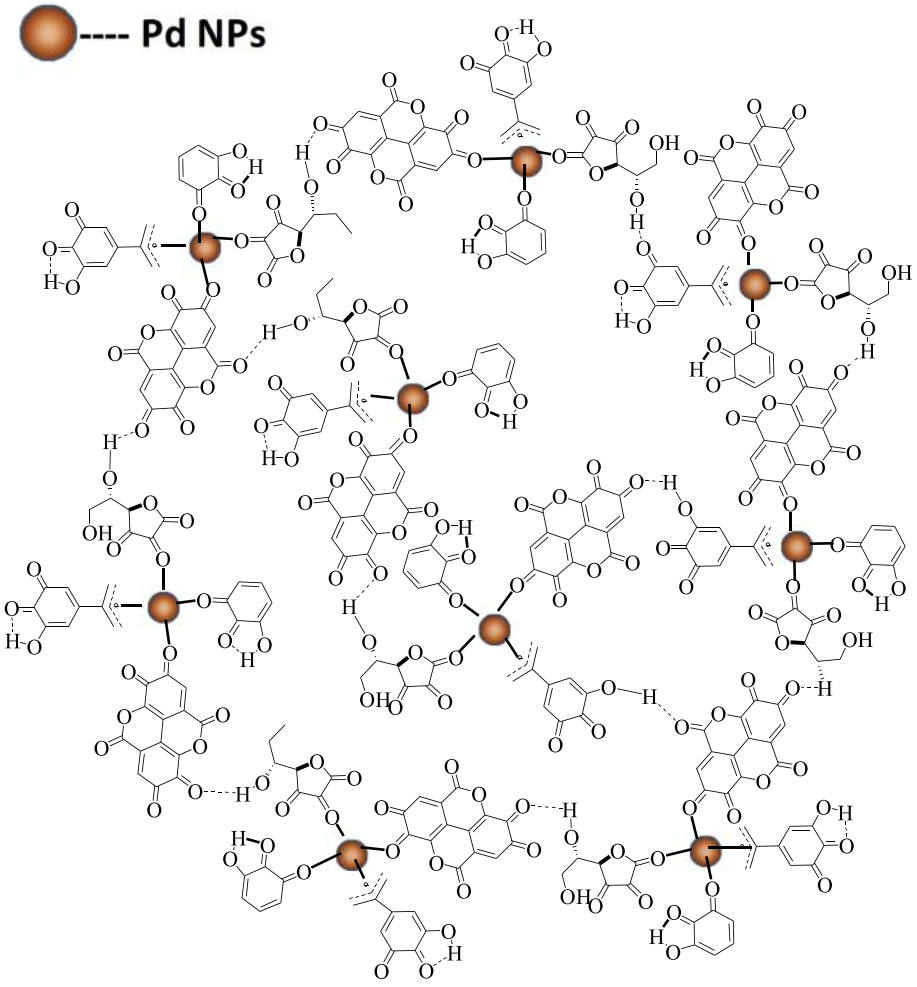


**Fig. 3** Schematic representation of phytochemicals based stabilization of Pd NPs.

erally the secondary metabolites i.e. polyphenols are good reducing and stabilizing agents. HPLC analysis of ECBP extract showed four major peaks with retention times of 2.27, 2.73, 3.23 and 3.66 min (Fig. S4) which correspond to ascorbic acid, gallic acid, pyrogallol and ellagic acid respectively after matching the corresponding reference standard compounds.

All the four identified water soluble phyto-constituents in the extracts with two hydroxyl (—OH) groups reduced metal ions to metal NPs (MNPs) and the corresponding quinone forms of phyto-constituents stabilized the synthesized Pd NPs via hydrogen bonding (Fig. 3) by transferring electron clouds around the carbonyl oxygen (—C═O) of oxidised poly-phenols to the surface of Pd NPs. Similar interaction between carbonyl oxygen atom and Pt NPs surface by *T. chebula* fruit extracts was reported earlier [43]. It is evident that all three oxidised polyphenols i.e. oxidised forms of ellagic acid, ascorbic acid and pyrogallol as well as the electrostatic interaction of oxidised form of gallic acid ($COO^{\overline{}}$) onto the surface of the Pd NPs caused stabilization of Pd NPs via inter- and intramolecular hydrogen bonding (Fig. 3). Also, hard soft–acid base (HSAB) concept played the key role in this stabilization process. Normally, polyphenols with at least three hydroxyl groups behave as hard ligands which do not make complex with soft palladium metal ions due to HSAB principle whereas Pd NPs being soft ligands make coordination bond with oxidised form of polyphenols i.e. the respective quinone forms as soft ligands followed by enhancement of stabilization.

Fig. 4A–F demonstrates the HR-TEM, SAED, EDAX and particles histogram of synthesized Pd NPs. Fig. 4A–C illustrates TEM images of Pd NPs at different magnification i.e. at (A) 30 nm, (B) 100 nm, (C) 200 nm and the majority of NPs was within the size range of 4–20 nm with a mean particles size of 12 nm which matches XRD results. A similar result was reported by Anand et al. [44] where Pd NPs size was within 16 to 20 nm. Fig. 4(D) shows the SAED pattern of Pd NPs and the bright spots in the form of circular rings indicate polycrystalline nature of Pd NPs. Fig. 4E shows the particles size histogram of Pd NPs and most of the NPs are between 10 and 15 nm. Also, Fig. 4F shows the elemental composition of Pd NPs obtained from the energy dispersive X-ray spectroscopy (EDAX) study which suggests the presence of Pd atoms (atomic percentage 75.40% and atomic weight percentage 64.67%) and remaining atomic peaks in SAED pattern are due to cupper grid which confirm its purity.

### *3.1. Catalytic activity of Pd NPs to reduction of azo-dyes*

The reduction of azo-dyes is more important for the waste water treatment and removal of textile colour from manufac-

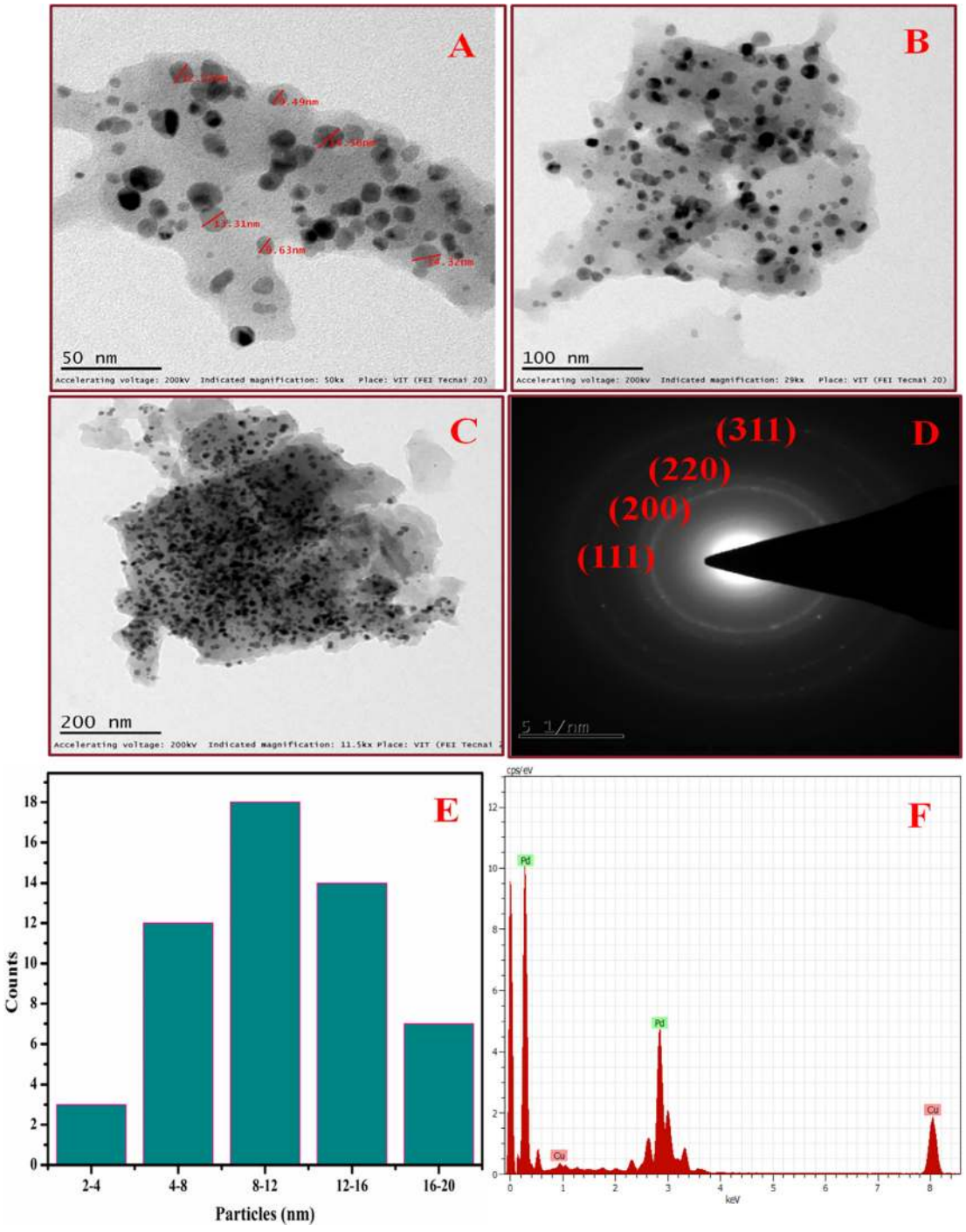


**Fig. 4** TEM images of synthesized Pd NPs at different magnification 50 nm (A), 100 nm (B), 200 nm (C), SAED pattern of Pd NPs (D), Particles size distribution of Pd NPs (E) and EDX spectrum of Pd NPs (F).

turing industry is a major environmental concern [45]. The synthesized Pd NPs having high surface area to volume ratio, reduced pollutants azo-dyes such as Sunset yellow, Methyl Orange, Tartrazine and Congo red dyes in dose dependent manner. Congo red (CR), a represented azo-dye with molecular formula of $C_{32}H_{22}N_6Na_2O_6S_2$, is a toxic and non-biodegradable dye originating from dyeing industries. It gives an absorption peak at 496 nm by UV–visible spectroscopy. Initially azo-dye CR was treated with $NaBH_4$ and almost no degradation was observed until 50 min of exposure (Fig. 5A). Then the degradation of CR was checked with $NaBH_4$ as electron donor and Pd NPs as catalyst (Fig. 5B). The progress of dye reduction was monitored by UV–visible spectroscopy at 496 nm with time. Also, Congo red dye solution was kept in dark without $NaBH_4$ and Pd NPs as blank to check whether it reduced or not. Our study results demonstrate that CR dye was reduced completely within 14 min (Fig. 5B). Catalytic efficiency of Pd NPs to CR dye reduction

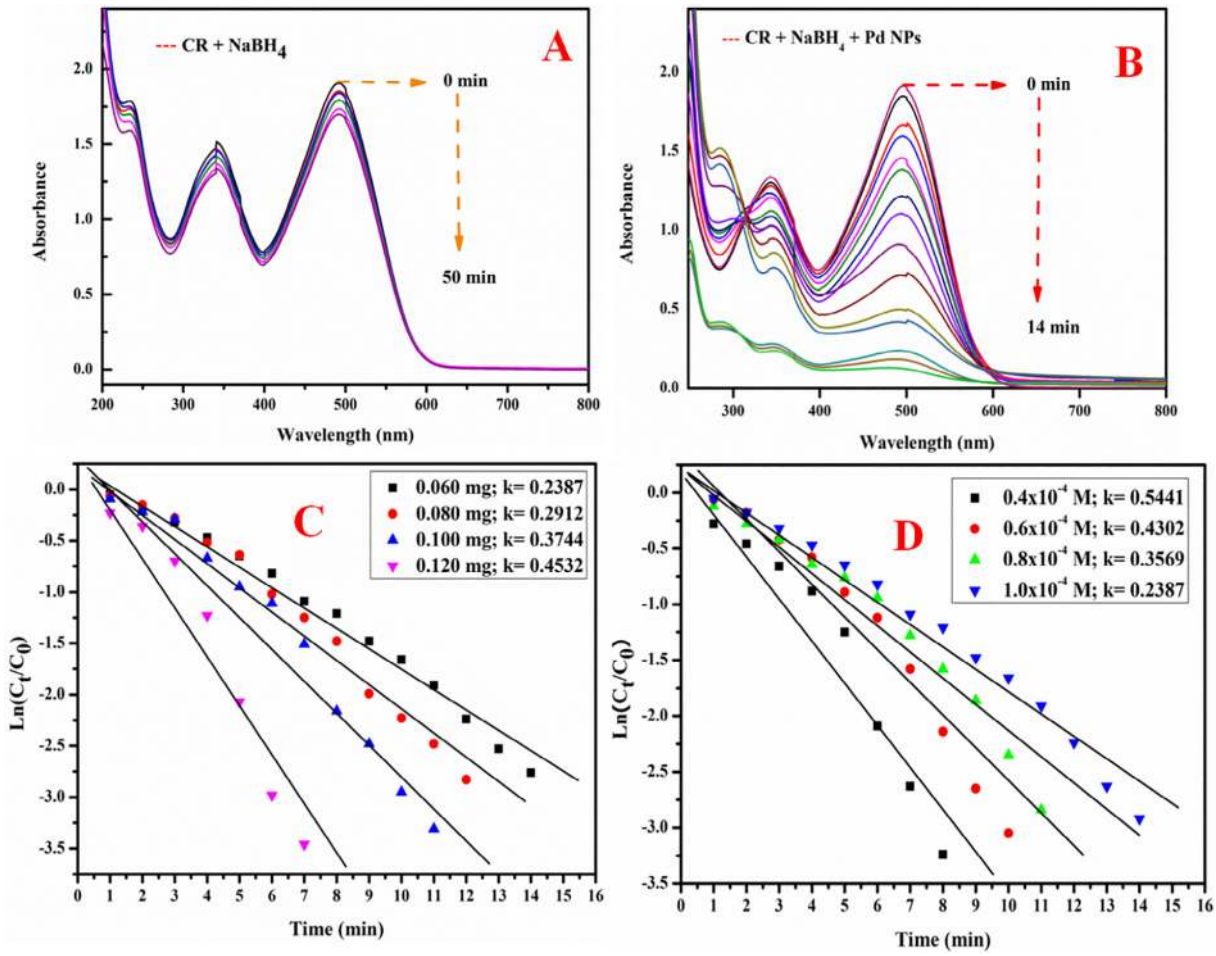


**Fig. 5** UV–Vis absorption spectra for the reduction of Congo Red dye by $NaBH_4$ aqueous solution without catalyst Pd NPs (A), with catalyst Pd NPs (B), Effect of Pd NPs doses (mg) on the reduction kinetics of Congo Red dye (C) and Effect of Congo Red dye concentration (M) on reduction kinetics of Congo Red dye at constant dose of catalyst Pd NPs (D).

was calculated by using the formula as "Reduction (%) = $(A_0-A_t)*100/A_0$, where $A_0$ is the absorbance of Congo red dye solution at zero time of exposure, $A_t$ is the absorbance of Congo red dye solution after time "t" of exposure. The calculated reduction efficiency (%) of Pd NPs to CR was 95.32%. Similar way the reduction of Congo red dye was reported by Kolya et al. [46]. As per Ismail et al. [47] reduction of nitrophenols and organic dyes degradation in the presence of plant supported Cu-Ag and Cu-Ni bimetallic NPs were promising.

Ismail et al. [48] reported zerovalent copper nanoparticles catalysed reduction of MO and Congo red by $NaBH_4$, whereas MO dye was reduced to low molecular free amino group compounds (hydrazine derivative) by $NaBH_4$ with the appearance of an absorption band at 468 nm. Mirzadeh et al. [49] reported the decolourization of Acid blue 25 and Acid orange 7 dyes by using biocatalyst (immobilized laccase of *P. variabile* on porous beads). Thermodynamically the redox potential difference between electron donor $NaBH_4$ and electron acceptor azo-dyes is huge, but in the presence of Pd NPs activation energy of dye and Pd NPs adduct is reduced significantly leading to kinetically favourable process i.e. rapid reduction of azo-dyes. Basically Pd NPs behaved as the carrier of electrons or helped electron shuttling process by passing off the electrons from donor $NaBH_4$ to the acceptor dye molecules [50].

### *3.2. Effect of catalyst dose and concentration of dye on reduction of Congo red dye*

The effect of Pd NPs catalyst dose on reduction of Congo red dye was checked by varying different doses of catalyst to a fixed concentration of dye (Fig. 5C). It clearly shows that the value of rate constant (0.2387–0.4532 $min^{-1}$) increased with increasing catalyst dose (0.06–0.12 mg) which supported the results of Omidvar et al. [51]. Similarly Bazrafshan et al. [52] reported increased catalyst (single walled carbon nanotubes) dose (0.01–0.05 g/L) for degradation of Reactive red-120 dye and percentage of dye degradation was increased with catalyst dose (Max ~ 88.28%). The catalytic reduction of Congo red followed the pseudo-first order kinetics and its kinetics equation is expressed as "ln $(C_t) = -k_t + \ln(C_0)$, where, $C_0$ is initial concentration of Congo red dye, $C_t$ is the concentration of the Congo red dye after reduction for time 't', and k is the rate constant. Fig. 5(C) represents the plot of ln $(C_t/C_0)$ vs. irradiation time (min) for the Congo red dye reduction with a linear relationship. It clearly shows that the value of rate constant increased with catalyst dose, whereas increasing amount of dye concentration at constant catalyst dose leads to decreasing rate constant (0.5441–2387 $min^{-1}$) (Fig. 5D). In similar way Wang et al. [53] reported the reduction of Cr(VI) to Cr(III)

by the generated $H_2O_2$ and also degradation of bisphenol A using $N_2$-g-$C_3N_4$, irradiation with visible light.

### 3.3. Catalytic activity of Pd NPs to reduction of Sunset Yellow dye

Sunset Yellow is an azo-dye, having conjugated aromatic rings with azo-bond and molecular formula as $C_{16}H_{10}N_2Na_2O_7S_2$. The reduction of Sunset yellow by $NaBH_4$ using catalyst Pd NPs was monitored by UV–visible spectroscopy at 485 nm. Fig. 6A shows the reduction progress of Sunset yellow dye with $NaBH_4$ and Pd NPs catalyst within 200–800 nm and it reduced almost completely within 9 min, whereas Fig. 6B shows kinetics of Pd NPs catalysed reduction of Sunset yellow. In the present study Sunset yellow was reduced by 97.19% within 9 min. Earlier Aliabadi et al. [54] reported removal of azo-dye Sunset yellow by polypyrrole, polyaniline NPs and nanocomposites, whereas Deepika et al. [55] reported photocatalytic degradation of Sunset yellow dye by using *Ailanthus excels* leaf and bark extract which supports our findings.

### 3.4. Catalytic activity of Pd NPs to reduction of Methyl Orange dye

Catalytic reduction of azo-dye MO ($C_{14}H_{14}N_3NaO_3S$) was monitored by measuring absorbance at 462 nm using UV–visible spectrophotometer. In the presence of electron donor $NaBH_4$ MO was reduced catalytically by Pd NPs with time. The progress of reduction is shown in Fig. 6C and it was reduced completely within 11 min. Fig. 6D show the kinetics of MO dye reduction and it was reduced by 96.37% with 11 min. Momeni et al. [56] reported the degradation of organic dye (Congo red, Methylene blue) by *Euphorbia prolifera* leaf extract mediated Cu/ZnO NPs. Kalathil et al. [57] studied the reduction of methyl orange dye in the presence of solid Pd/Hollow Pd NPs. The reduction potential of methyl orange c-Cyts (outer-membrane c-type cytochromes) is ′0.150 V (vs. Ag/AgCl) while for $Pd^{2+}$/Pd metal is + 0.787 (vs. Ag/AgCl). Here, the reduction potential of the Pd is more positive than the OM c-Cyts and hence electron transfer from the MO c-Cyts to the Pd NPs was preferred. Eventually the electrons captured by the Pd NPs reduced the adsorbed dye on its surfaces. In addition, Lebaschi et al. [58] used Pd NPs (which was prepared by tea leaf extract) for the reduction of 4-nitro phenol to 4-nitro amine. All these results supported our results.

### 3.5. Catalytic activity of Pd NPs to reduction of Tartrazine dye

The catalytic activity of synthesized Pd NPs for the reduction of azo-dye Tartrazine ($C_{16}H_9N_4Na_3O_9S_2$) was investigated in aqueous medium by measuring absorbance at 414 nm. Fig. 6E shows the reduction of Tartrazine dye with time and it was reduced by 96.09% within 12 min (Fig. 6F). A possible mechanism of dye reduction is illustrated in Fig. 7 for Sunset yellow and Tartrazine and for methyl Orange and Congo red in Fig. 8. It is clear that Pd NPs reduced activation energy barrier being as carrier of electrons and led to rapid reduction by increasing rate constant value. Other methods also used to remove these dyes from the environment e.g. Banerjee et al. [59] used low cost agro-materials as adsorbent for the removal of toxic Tartrazine dye by batch mode adsorption, while Naama et al. [60] used silicon nano-wires with metal NPs for photocatalytic degradation of Tartrazine dye and Gulen Tekin et al. [61] used photo-Fenton oxidation with bismuth oxyhalide catalyst for degradation of tartrazine dye.

Tables (1, ST1) summarize results on reduction of CR, MO by $NaBH_4$ (Table 1) and photodegradation of TZ and SY by UV light irradiation catalysed by different NPs (Table ST1) [62–76]. It clearly shows that the catalytic efficiency of different NPs towards degradation of dyes depends on their doses, sizes and shapes (Table 1) [62–68] and in the presence of UV light (Table ST1) [69–76]. Pure spherical shaped Ag NPs having mean diameter within 2.7–35 nm catalytically degraded Congo red by 100% within 10–240 min [62,63,65] and 24 nm spherical Ag/$TiO_2$ NPs degraded 100% in 30 sec [63], whereas spherical Pd NPs with a mean diameter of 12 nm degraded 95.3% in 14 min in the presence of $NaBH_4$ (Table 1). Although Ag/$TiO_2$ NPs degraded within 30 sec, its amount of NPs (μg) to amount of dye (μm) was 19.9 [64], but in our study CR dye was reduced within 14 min with a ratio of NPs to dye as 0.29. Hence the present study utilised minimum amount of Pd NPs for 95% reduction of CR dye (Table 1).

For the degradation of MO many researchers have used pure Ag NPs [67,68], Ag/$TiO_2$ NPs [64], Pd/sodium borosilicate NPs [65] and pure Pd NPs [Present study] in the presence of reducing agent $NaBH_4$ (Table 1). With respect to amount of catalyst (μg) to amount of dye (μg) ratio and degradation time Pd/sodium borosilicate NPs degraded MO by about 95% in 3.8 min with ratio of catalyst to dye as 20.4, but our Pd NPs catalyst with a ratio of catalyst to dye as 0.61 reduced 96.4% in 11 min (Table 1). These results clearly indicate that the synthesized Pd NPs is highly capable to reduce MO in a shorter time with minimum catalytic dose in the presence of a reducing agent such as $NaBH_4$.

Several reports have utilized semiconducting nanomaterials such as ZnO [69], $TiO_2$ [70] and $TiO_2$/MRGO [71], CdS [72] (PVP-Capped) for photodegradation of Tartrazine (TZ) dye under UV irradiation except our study where Pd NPs along with $NaBH_4$ as reducing agent was used for degradation of TZ dye (Table ST1). With respect to nanocatalyst (mg) to dye (mg) ratio our study used very low amount nanocatalyst [i.e. catalyst (mg)/dye (mg) ratio as 0.37] when compared to others (~2.5 to 18.7) (Table 1) which clearly indicates that Pd NPs catalysed very strongly in reducing TZ dye in the presence of $NaBH_4$ as reducing agent within 12 min compared to others in hr.

Sunset yellow (SY) dye is used in different food processing industries. Many researchers have used different nanomaterials such as Cu-loaded bentonite catalyst [73], ZnS/$TiO_2$ [74], $TiO_2$ /activated carbon [75], $TiO_2$-Pt/RGO [76] for the photodegradation of SY dye. It is clear that these catalysts took more than hour for photodegradation of SY dye under UV irradiation with catalyst (mg) to dye (mg) ratio of 22–92 (Table ST1), whereas our study used reducing agent $NaBH_4$ to reduce SY dye by Pd NPs as catalyst. Interestingly $NaBH_4$ reduced 97% SY dye with Pd NPs catalyst within 9 min at a catalyst to dye ratio of 0.44 which shows its superiority over other catalysts (Table ST1). Zhang et al. [77] proposed a possible mechanism for degradation of bisphenol A dye by using dual-oxygen-doped porous g-$C_3N_4$ photocatalyst.

Our study results show that CR was reduced within 14 min with a rate constant of 0.23875 $min^{-1}$, MR reduced within

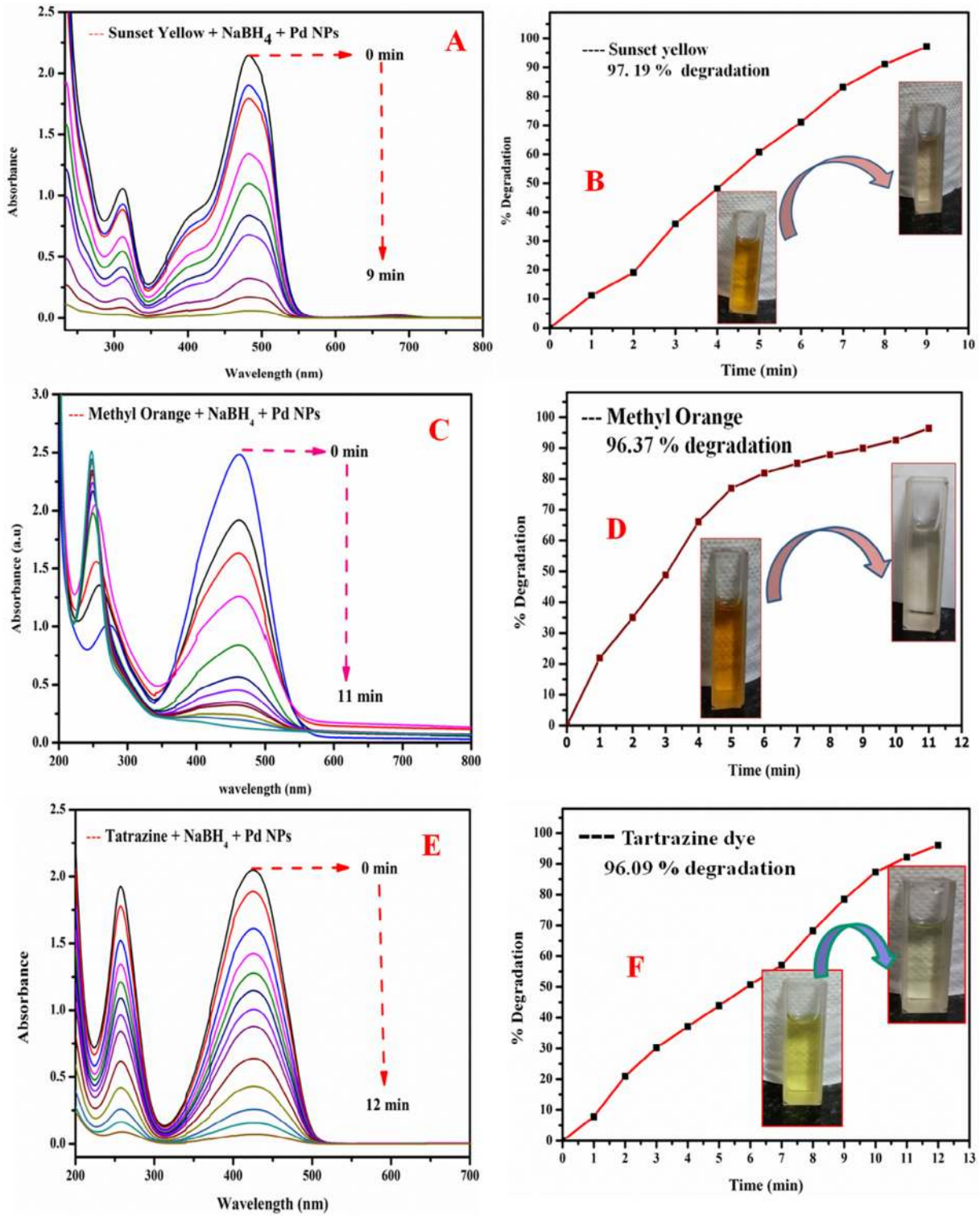


**Fig. 6** Reduction of Sunset Yellow (SY) (A), Methyl Orange (MO) (C), Tartrazine (TZ) (E) by $NaBH_4$ aqueous solution with catalyst Pd NPs and degradation kinetics of SY (%) (B), MO (%) (D) and TZ (%) (F) with time by $NaBH_4$ aqueous solution with catalyst Pd NPs.

11 min with a rate constant of 0.27675 $min^{-1}$ while TZ reduced within 12 min with a rate constant of 0.32765 $min^{-1}$, SY reduced within 9 min with the rate constant of 0.45223 $min^{-1}$, which suggests different catalytic activity of Pd NPs in the presence of $NaBH_4$ to individual dyes. In fact metallic NPs served as electron relays in a redox reaction where CR, MO, TZ and SY behaved as electrophile and $BH_4^-$ as nucleophile with respect to NPs (Figs. 7, 8). The nucleophile $NaBH_4$ donated an electron to Pd NPs and electrophiles i.e. dyes captured electrons via Pd NPs for reducing pollutants dyes. Con-

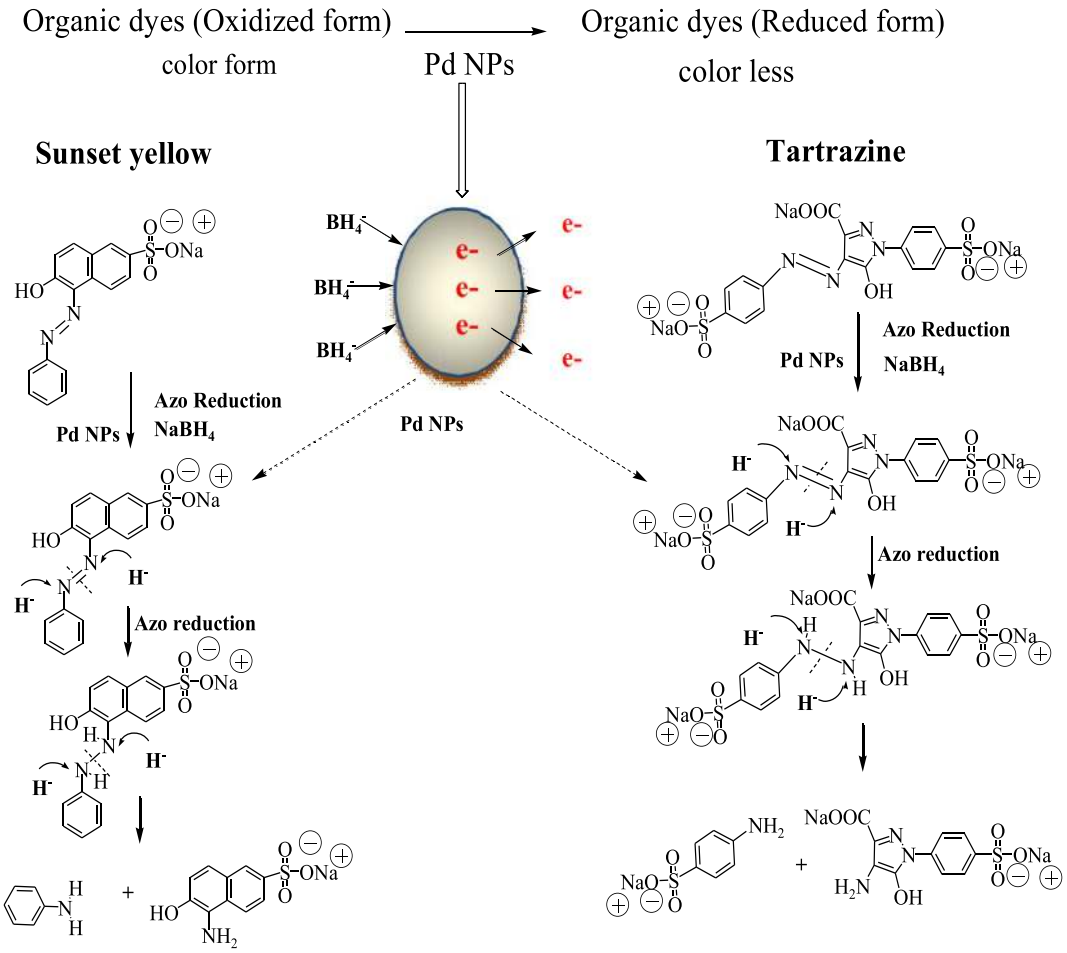


**Fig. 7** Plausible mechanism for the reduction of Sunset Yellow and Tartrazine dyes by $NaBH_4$ aqueous solution with catalyst Pd NPs.

sequently the synthesized Pd NPs reduced activation energy of the dye-Pd NPs adducts and could be an efficient catalyst in reducing pollutants dyes at a faster rate. Rostami-Vartooni et al. [78] proposed a possible mechanism of methyl orange and 4-NPs reduction by $NaBH_4$ with $Ag/Fe_3O_4$/HZSM catalyst.

### *3.6. Recyclability and stability study of Pd nanoparticles*

The recyclability of the recovered Pd NPs was investigated for the reduction of CR, MO and SY, TZ. In first cycles 3 mL of Congo red (1x10-4) was mixed with 150 μL (0.05 M) freshly prepared NaBH4 and then 60 μL of Pd NPs colloidal solution (1 μg/μL) was added to carry out the reaction process and after completion reduction of dye, the catalyst was collected through the centrifugation and supernatant was monitored by UV–visible spectroscopy. For the second cycle the residue was added to 3 mL dye and then sonicated upto complete dispersion of catalyst and then mixed with 150 μL (0.05 M) freshly prepared $NaBH_4$ and allowed for completion of the reaction. In similar way third and fourth cycles were carried out. The reduction of dye was almost similar during the recycling of the recovered Pd NPs catalyst i.e. the reduction efficiency of Congo red was 95.32%, 94.64%, 92.73%, 91.62% for 1st, 2nd, 3rd and 4th cycles respectively (Fig. 9A). Our result thoroughly resembled to the findings of Omidvar et al. [51]. The four-fold recycling test of Pd NPs catalyst was carried out for the reduction of Methyl orange (96.37%, 95.56%, 93.22%, 92.02%), Tartrazine (96.09%, 95.84%, 94.88%, 93.17%), and Sunset yellow (97.19%, 96.35%, 95.53% 94.02%) which are shown in Fig. 9(A). Pd NPs catalyst was collected to study the stability by using dynamic light scattering (DLS) study after fourth cycle of experiments. Fig. 9(B) show the zeta potential value of the recovered Pd NPs aqueous dispersion as −46.5 mV compare to as- synthesized Pd NPs zeta potential value of −62.5 mV. This study results suggest that even after fourth cycle Pd NPs are very highly stable. Bincy Rose Vergis et al. [79] reported methylene blue dye degradation by sung $ZnFe_2O_4$ nanomaterials and there was slight decrease in its efficiency after 4 cycles (i.e. degradation efficiency decreased from 73% to 54%). Also, Mangalam et al. [80] reported azo dye (methyl orange) degradation by using silver/reduced graphene oxide (Ag/rGO) nanocomposite where the photocatalytic activity of Ag/rGO nanocomposite remained almost 90% upto three cycles. The plausible mechanism for reduction of azo dyes by $NaBH_4$ with Pd NPs as catalyst is schematically presented in Fig. 9(C).

In summary it is clear that Pd NPs behaves as a carrier of electrons which allows hydride ions participation in cleaving

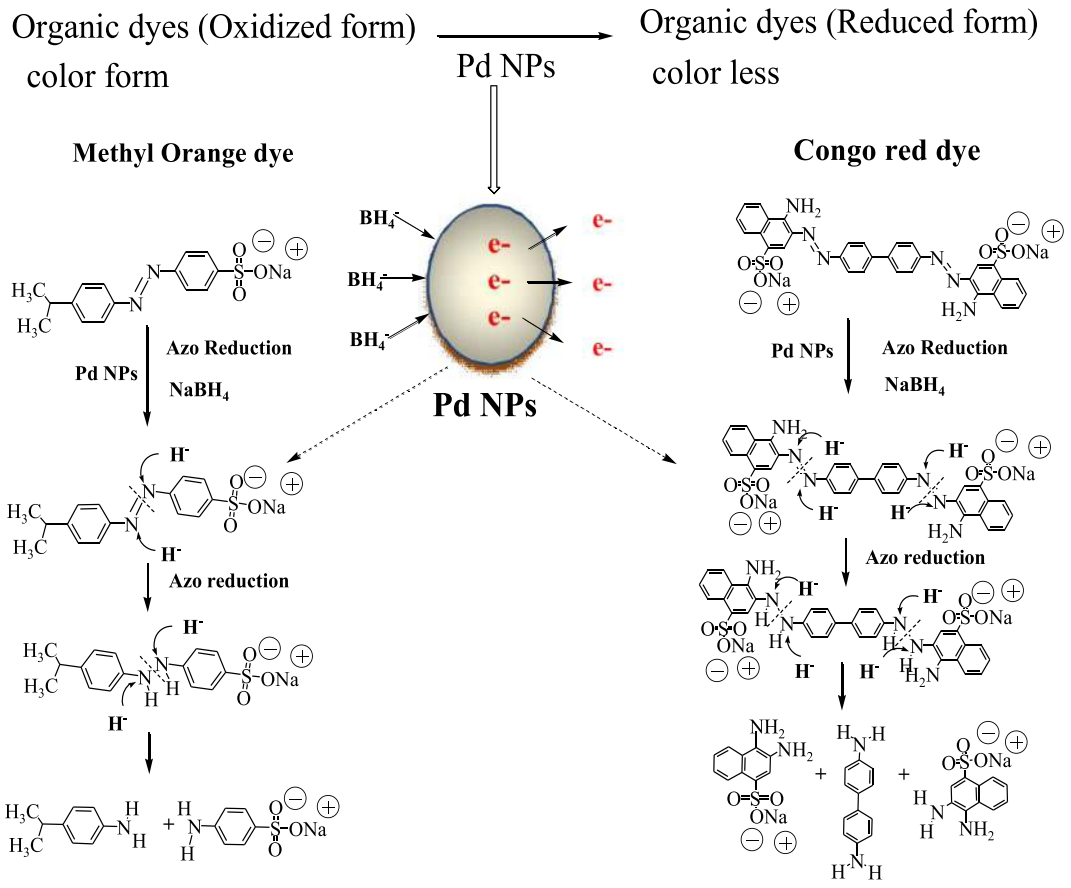


**Fig. 8** Plausible mechanism for the reduction of Methyl Orange and Conge Red by $NaBH_4$ aqueous solution with Pd NPs as catalyst.

**Table 1** Catalytic activity comparison of Pd NPs on reduction of Congo red (CR), Methyl Orange (MO), Tartrazine (TZ) and Sunset yellow (SY) dyes in the presence of $NaBH_4$.

| Dye | NPs | NPs(μg)/dye (μg) | Mean Size (nm)/shape | Time (min) | Degradation (%) | Ref. |
|---|---|---|---|---|---|---|
| CR | Ag NPs | 239 | 35 nm/spherical | 240 | 100 | [62] |
| | Ag NPs | 227.7 | 25 nm/spherical | 45 | ~ 85 | [63] |
| | Ag/$TiO_2$ | 19.93 | 24 nm/spherical | 0.5 | 100 | [64] |
| | Ag NPs | 10.52 | 2.67 nm/spherical | 10 | ~95 | [65] |
| | Pd NPs | 0.29 | 12 nm/spherical | 14 | 95.32 | Present work |
| MO | Ag/$TiO_2$ NPs | 40.74 | 24 nm/spherical | 9 | 100 | [64] |
| | Pd/sodium borosilicate | 20.37 | 20 nm/spherical | 3.8 | ~95 | [66] |
| | Ag NPs | 20.37 | 11 nm/sheet shape | 11 | 100 | [67] |
| | Ag NPs | 0.11 | 30 nm/spherical | 60 | ~37 | [68] |
| | Pd NPs | 0.61 | 12 nm/spherical | 11 | 96.37 | Present work |
| TZ | Pd NPs | 0.36 | 12 nm/spherical | 12 | 96.09 | Present work |
| SY | Pd NPs | 0.44 | 21 nm/Spherical (from XRD) | 9 | 97.19 | Present work |

azo-bond of azo-dyes and resulting to nontoxic smaller fragments. When the nano-catalyst is added to the reaction mixture, it helps in the electron-shuttling process by passing off the electrons to the dye molecules from $NaBH_4$ as donor via mediator Pd nano-catalyst i.e. electrons from $NaBH_4$ moves via Pd NPs as mediator and forms hydride ions which cleaves dyes to non-toxic species, eventually the absorption of azo-dye intensity vanishes within the specified time.

## 4. Conclusion

In this present work Pd NPs was synthesized by ECBP aqueous extract and the synthesized Pd NPs were characterized by UV–Vis, XRD, TEM and EDX. The highly stable spherical Pd NPs was used for catalytic reduction of the azo-dyes CR, MO, SY and TZ by $NaBH_4$. The reduction of organic azo-dyes was 95–97% within 14 min. Hence, Pd NPs could be

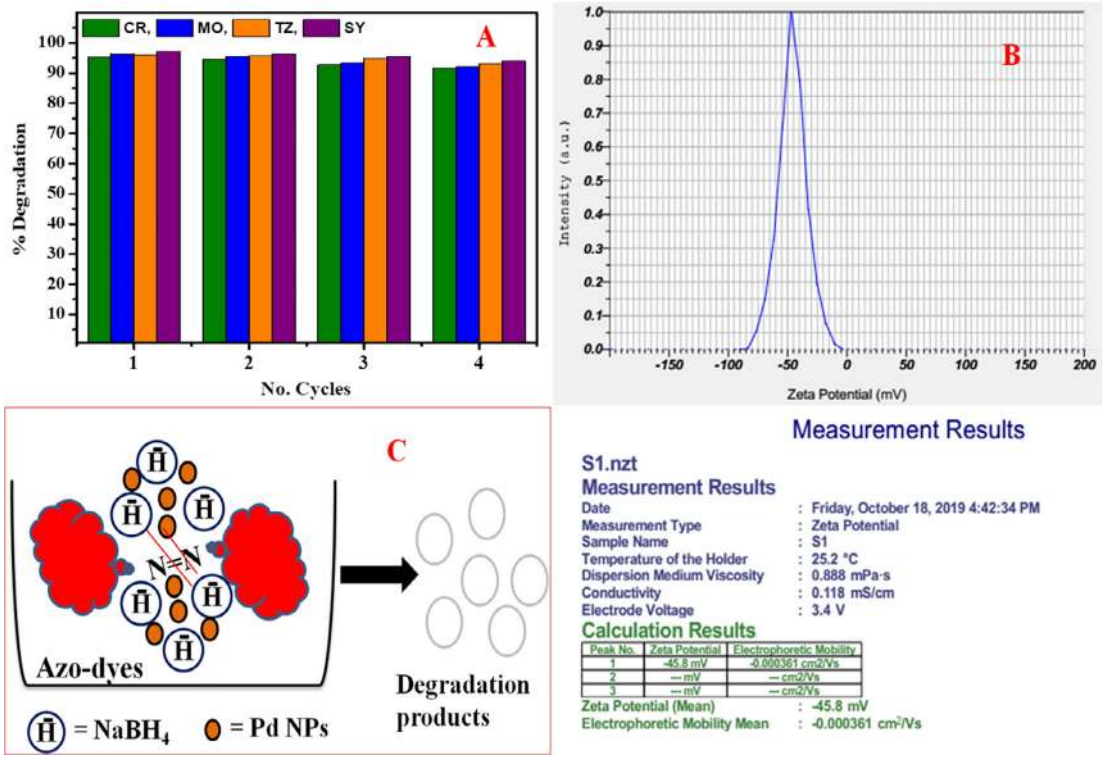


**Fig. 9** The catalytic efficiency of Pd NPs for reduction of CR, MO, TZ and SY (A), Zeta potential analysis of Pd NPs collected after reduction by DLS study (B) and Possible mechanism of azo dye reduction by $NaBH_4$ as reducing agent and Pd NPs as catalyst (C).

the promising catalyst in the reduction/degradation of organic azo-dyes.

## Declaration of Competing Interest

The authors declare that they have no known competing financial interests or personal relationships that could have appeared to influence the work reported in this paper.

## Acknowledgements

The authors thank Vellore Institute of Technology, Vellore for the financial support, working platform and instrumental facility given to complete the study. Especially, the authors thank VIT for providing "VIT SEED GRANT" for carrying out this research work.

## Appendix A. Supplementary data

Supplementary data to this article can be found online at https://doi.org/10.1016/j.jscs.2019.11.003.

## References

[1] P.M. Uberman, C.S. García, J.R. Rodríguez, S.E. Martín, PVP-Pd nanoparticles as efficient catalyst for nitroarene reduction under mild conditions in aqueous media, Green Chem. 19 (2017) 739–748.
[2] E. Bazrafshan, M.R. Alipour, A.H. Mahvi, Textile wastewater treatment by application of combined chemical coagulation, electrocoagulation, and adsorption processes, Desalin. Water Treat. 57 (2016) 9203–9215.
[3] M.S. Abdel-Aziz, M.S. Shaheen, A.A. El-Nekeety, M.A. Abdel-Wahhab, Antioxidant and antibacterial activity of silver nanoparticles biosynthesized using Chenopodium murale leaf extract, J. Saudi Chem. Soc. 18 (2014) 356–363.
[4] R. Lakshmipathy, B. Palakshi Reddy, N.C. Sarada, K. Chidambaram, S. Khadeer Pasha, Watermelon rind-mediated green synthesis of noble palladium nanoparticles: catalytic application, Appl. Nanosci. 5 (2015) 223–228.
[5] V.S. Coker, J.A. Bennett, N.D. Telling, T. Henkel, J.M. Charnock, G. van der Laan, R.A.D. Pattrick, C.I. Pearce, R. S. Cutting, I.J. Shannon, J. Wood, E. Arenholz, I.C. Lyon, J.R. Lloyd, Microbial engineering of nanoheterostructures: biological synthesis of a magnetically recoverable palladium nanocatalyst, ACS Nano 4 (2010) 2577–2584.
[6] H. Wang, Y. Liu, M. Li, H. Huang, H.M. Xu, R.J. Hong, H. Shen, Diastase assisted green synthesis of size controllable gold nanoparticles, Optoelectron. Adv. Mater. Rapid Commun. 4 (2010) 1166–1169.
[7] T. Mori, T. Hegmann, Determining the composition of gold nanoparticles: a compilation of shapes, sizes, and calculations using geometric considerations, J. Nanoparticle Res. 18 (2016) 1–36.
[8] M. Pálmai, E.M. Zahran, S. Angaramo, S. Bálint, Z. Pászti, M. R. Knecht, L.G. Bachas, Pd-decorated m-$BiVO_4$/BiOBr ternary composite with dual heterojunction for enhanced photocatalytic activity, J. Mater. Chem. A 5 (2017) 529–534.
[9] M. Eslamian, M. Shekarriz, Recent advances in nanoparticle preparation by spray and microemulsion methods, Recent Pat. Nanotechnol. 3 (2009) 99–115.
[10] S. Shamaila, A.K.L. Sajjad, N. ul A. Ryma, S.A. Farooqi, N. Jabeen, S. Majeed, I. Farooq, Advancements in nanoparticle

fabrication by hazard free eco-friendly green routes, Appl. Mater. Today 5 (2016) 150–199.
[11] S. Joseph, B. Mathew, Facile synthesis of silver nanoparticles and their application in dye degradation, Mater. Sci. Eng. B 195 (2015) 90–97.
[12] Q. Huang, S. Song, Z. Chen, B. Hu, J. Chen, X. Wang, Biochar-based materials and their applications in removal of organic contaminants from wastewater: state-of-the-art review, Biochar 1 (2019) 45–73.
[13] S. Ahmed, Annu, S.A. Chaudhry, S. Ikram, A review on biogenic synthesis of ZnO nanoparticles using plant extracts and microbes: a prospect towards green chemistry, J. Photochem. Photobiol. B Biol. 166 (2017) 272–284.
[14] V. Sai Saraswathi, J. Tatsugi, P.K. Shin, K. Santhakumar, Facile biosynthesis, characterization, and solar assisted photocatalytic effect of ZnO nanoparticles mediated by leaves of L. speciosa, J. Photochem. Photobiol. B Biol. 167 (2017) 89–98.
[15] B. Ajitha, Y.A. Kumar, S. Shameer, K.M. Rajesh, Y. Suneetha, P.S. Reddy, Lantana camara leaf extract mediated silver nanoparticles: antibacterial, green catalyst, J. Photochem. Photobiol. B Biol. 149 (2015) 84–92.
[16] J. Jeevanandam, Y.S. Chan, M.K. Danquah, Biosynthesis of metal and metal oxide nanoparticles, Chem. Bio. Eng. Rev. 3 (2016) 55–67.
[17] M. Khan, G.H. Albalawi, M.R. Shaik, M. Khan, S.F. Adil, M. Kuniyil, H.Z. Alkhathlan, A. Al-Warthan, M.R.H. Siddiqui, Miswak mediated green synthesized palladium nanoparticles as effective catalysts for the Suzuki coupling reactions in aqueous media, J. Saudi Chem. Soc. 21 (2016) 450–457.
[18] A. Kalaiselvi, S.M. Roopan, G. Madhumitha, C. Ramalingam, G. Elango, Synthesis and characterization of palladium nanoparticles using Catharanthus roseus leaf extract and its application in the photo-catalytic degradation, Spectrochim. Acta - Part A Mol. Biomol. Spectrosc. 135 (2015) 116–119.
[19] S. Zhang, P. Gu, R. Ma, C. Luo, T. Wen, G. Zhao, W. Cheng, X. Wang, Recent developments in fabrication and structure regulation of visible-light-driven g-$C_3N_4$-based photocatalysts towards water purification: a critical review, Catal. Today 335 (2019) 65–77.
[20] F. Gholami-Borujeni, A.H. Mahvi, S. Nasseri, M.A. Faramarzi, R. Nabizadeh, M. Alimohammadi, Enzymatic treatment and detoxification of acid orange 7 from textile wastewater, Appl. Biochem. Biotechnol. 165 (2011) 1274–1284.
[21] B. Murugesan, J. Sonamuthu, S. Samayanan, S. Arumugam, S. Mahalingam, Highly biological active antibiofilm, anticancer and osteoblast adhesion efficacy from MWCNT/PPY/Pd nanocomposite, Appl. Surf. Sci. 434 (2018) 400–411.
[22] A. Balbín, F. Gaballo, J. Ceballos-Torres, S. Prashar, M. Fajardo, G.N. Kaluđerović, S. Gómez-Ruiz, Dual application of Pd nanoparticles supported on mesoporous silica SBA-15 and MSU-2: supported catalysts for C-C coupling reactions and cytotoxic agents against human cancer cell lines, RSC Adv. 4 (2014) 54775–54787.
[23] S. Zhang, S. Song, P. Gu, R. Ma, D. Wei, G. Zhao, T. Wen, R. Jehan, B. Hu, X. Wang, Visible-light-driven activation of persulfate over cyano and hydroxyl group co-modified mesoporous g-$C_3N_4$ for boosting bisphenol A degradation, J. Mater. Chem. A. 7 (2019) 5552–5560.
[24] M. Khalkhali, Q. Liu, H. Zeng, H. Zhang, A size-dependent structural evolution of ZnS nanoparticles, Sci. Rep. 5 (2015) 1–17.
[25] K. Mohan, B.K. Mandal, H.A. Kiran, Green synthesis of size controllable gold nanoparticles, Spectrochim. Acta Part A Mol. Biomol. Spectrosc. 116 (2013) 539–545.
[26] N.A. Youssef, S.A. Shaban, F.A. Ibrahim, A.S. Mahmoud, Degradation of methyl orange using Fenton catalytic reaction, Egypt. J. Pet. 25 (2016) 317–321.
[27] A. Rostami-Vartooni, M. Nasrollahzadeh, M. Alizadeh, Green synthesis of perlite supported silver nanoparticles using Hamamelis virginiana leaf extract and investigation of its catalytic activity for the reduction of 4-nitrophenol and Congo red, J. Alloy. Compd. 680 (2016) 309–314.
[28] R. Ma, S. Zhang, T. Wen, P. Gu, L. Li, G. Zhao, F. Niu, Q. Huang, Z. Tang, X. Wang, A critical review on visible-light-response $CeO_2$-based photocatalysts with enhanced photooxidation of organic pollutants, Catal. Today 335 (2019) 20–30.
[29] A. Dalvand, R. Nabizadeh, M.R. Ganjali, M. Khoobi, S. Nazmara, A.H. Mahvi, Modeling of Reactive Blue 19 azo dye removal from colored textile wastewater using L-arginine-functionalized $Fe_3O_4$ nanoparticles: optimization, reusability, kinetic and equilibrium studies, J. Magn. Magn. Mater. 404 (2016) 179–189.
[30] A. Rostami-Vartooni, M. Nasrollahzadeh, M. Salavati-Niasari, M. Atarod, Photocatalytic degradation of azo dyes by titanium dioxide supported silver nanoparticles prepared by a green method using Carpobrotus acinaciformis extract, J. Alloy. Compd. 689 (2016) 15–20.
[31] A. Hatamifard, M. Nasrollahzadeh, S.M. Sajadi, Biosynthesis, characterization and catalytic activity of an Ag/zeolite nanocomposite for base-and ligand-free oxidative hydroxylation of phenylboronic acid and reduction of a variety of dyes at room temperature, New J. Chem. 40 (2016) 2501–2513.
[32] P. Dauthal, M. Mukhopadhyay, Biofabrication, characterization, and possible bio-reduction mechanism of platinum nanoparticles mediated by agro-industrial waste and their catalytic activity, J. Ind. Eng. Chem. 22 (2015) 185–191.
[33] H. Qian, Q. He, J. Zheng, S. Li, S. Zhang, Catechol-functionalized microporous organic polymer as supported media for Pd nanoparticles and its high catalytic activity, Polymer 55 (2014) 550–555.
[34] H. Wang, H. Guo, N. Zhang, Z. Chen, B. Hu, X. Wang, Enhanced Photoreduction of U (VI) on $C_3N_4$ by Cr (VI) and Bisphenol A: ESR, XPS and EXAFS Investigation, Environ. Sci. Technol. 53 (2019) 6454–6461.
[35] M.N. Safdar, T. Kausar, S. Jabbar, A. Mumtaz, K. Ahad, A.A. Saddozai, Extraction and quantification of polyphenols from kinnow (Citrus reticulate L.) peel using ultrasound and maceration techniques, J. Food Drug Anal. 25 (2017) 488–500.
[36] S. Yihan, L. Mingming, Z. Guo, Ag nanoparticles loading of polypyrrole-coated superwetting mesh for on-demand separation of oil-water mixtures and catalytic reduction of aromatic dyes, J. Colloid Interface Sci. 527 (2018) 187–194.
[37] M.L. Xu, X.C. Wu, J.J. Zhu, Green preparation and catalytic application of Pd nanoparticles, Nanotech 19 (2008) 305603.
[38] M. Khan, M. Khan, M. Kuniyil, S.F. Adil, A. Al-Warthan, H. Z. Alkhathlan, W. Tremel, M.N. Tahir, M.R.H. Siddiqui, Biogenic synthesis of palladium nanoparticles using *Pulicaria glutinosa* extract and their catalytic activity towards the Suzuki coupling reaction, Dalt. Trans. 43 (2014) 9026–9031.
[39] M. Hazarika, D. Borah, P. Bora, A.R. Silva, P. Das, Biogenic synthesis of palladium nanoparticles and their applications as catalyst and antimicrobial agent, PloS One 12 (2017) 0184936.
[40] R.K. Petla, S. Vivekanandhan, M. Misra, A. Mohanty, N. Satyanarayana, Soybean (Glycine max) leaf extract based green synthesis of palladium nanoparticles, J. Biomater. Nanobiotechnol. 3 (2012) 14–19.
[41] N. Basavegowda, K. Mishra, Y.R. Lee, S.H. Kim, Antioxidant and anti-tyrosinase activities of palladium nanoparticles synthesized using Saururus chinensis, J. Clust. Sci. 27 (2016) 733–744.
[42] A. Rostami-Vartooni, Green synthesis of CuO nanoparticles loaded on the seashell surface using Rumex crispus seeds extract

and its catalytic applications for reduction of dyes, IET Nanobiotechnol. 11 (2016) 349–359.
[43] K.M. Kumar, B.K. Mandal, S.K. Tammina, Green synthesis of nano platinum using naturally occurring polyphenols, RSC Adv. 3 (2013) 4033–4039.
[44] K. Anand, C. Tiloke, A. Phulukdaree, B. Ranjan, A. Chuturgoon, S. Singh, R.M. Gengan, Biosynthesis of palladium nanoparticles by using Moringa oleifera fl ower extract and their catalytic and biological properties, J. Photochem. Photobiol. B Biol. 165 (2016) 87–95.
[45] B. Mao, A. Qingda, B. Zhai, Z. Xia, S. Zhai, Multifunctional hollow polydopamine-based composites ($Fe_3O_4$/PDA@Ag) for efficient degradation of organic dyes, RSC Adv. 6 (2016) 47761–47770.
[46] H. Kolya, P. Maiti, A. Pandey, T. Tripathy, Green synthesis of silver nanoparticles with antimicrobial and azo dye (Congo red) degradation properties using Amaranthus gangeticus Linn leaf extract, J. Anal. Sci. Technol. 6 (2015) 33.
[47] M. Ismail, M.I. Khan, S. Bahadar, M. Ali, K. Akhtar, A.M. Asiri, Green synthesis of plant supported Cu-Ag and Cu-Ni bimetallic nanoparticles in the reduction of nitrophenols and organic dyes for water treatment, J. Mol. Liq. 260 (2018) 78–91.
[48] M. Ismail, S. Gul, M.I. Khan, M.A. Khan, A.M. Asiri, S.B. Khan, Green synthesis of zerovalent copper nanoparticles for efficient reduction of toxic azo dyes congo red and methyl orange, Green Process. Synth. 8 (2019) 135–143.
[49] S.S. Mirzadeh, S.M. Khezri, S. Rezaei, H. Forootanfar, A.H. Mahvi, M.A. Faramarzi, Decolorization of two synthetic dyes using the purified laccase of Paraconiothyrium variabile immobilized on porous silica beads, J. Environ. Health Sci. Eng. 12 (2014) 6.
[50] M. Nasrollahzadeh, M. Atarod, B. Jaleh, M. Gandomirouzbahani, In situ green synthesis of Ag nanoparticles on graphene oxide/$TiO_2$ nanocomposite and their catalytic activity for the reduction of 4-nitrophenol, congo red and methylene blue, Ceram. Int. 42 (2016) 8587–8596.
[51] A. Omidvar, B. Jaleh, M. Nasrollahzadeh, H.R. Dasmeh, Fabrication, characterization and application of GO/$Fe_3O_4$/Pd nanocomposite as a magnetically separable and reusable catalyst for the reduction of organic dyes, Chem. Eng. Res. Des. 121 (2017) 339–347.
[52] E. Bazrafshan, F.K. Mostafapour, A.R. Hosseini, A.R. Khorshid, A.H. Mahvi, Decolorisation of reactive red 120 dye by using single-walled carbon nanotubes in aqueous solutions, J. Chem. 2013 (2012) 938374.
[53] H. Wang, Q. Li, S. Zhang, Z. Chen, W. Wang, G. Zhao, L. Zhuang, B. Hu, X. Wang, Visible-light-driven $N_2$-g-$C_3N_4$ as a highly stable and efficient photocatalyst for bisphenol A and Cr (VI) removal in binary systems, Catal. Today 335 (2019) 110–116.
[54] R.S. Aliabadi, N.O. Mahmoodi, Synthesis and characterization of polypyrrole, polyaniline nanoparticles and their nanocomposite for removal of azo dyes; sunset yellow and Congo red, J. Clean. Prod. 179 (2018) 235–245.
[55] S. Deepika, R. Harishkumar, M. Dinesh, R. Abarna, Photocatalytic degradation of synthetic food dye, sunset yellow FCF (FD & C yellow no.6) by Ailanthus excelsa Roxb. possessing antioxidant and cytotoxic activity, J. Photochem. Photobiol., B Biol. 177 (2017) 44–55.
[56] S.S. Momeni, M. Nasrollahzadeh, A. Rustaiyan, Green synthesis of the Cu/ZnO nanoparticles mediated by Euphorbia prolifera leaf extract and investigation of their catalytic activity, J. Colloid Interface Sci. 472 (2016) 173–179.
[57] S. Kalathil, R. Chaudhuri, Hollow palladium nanoparticles facilitated biodegradation of an azo dye by electrically active biofilms, Materials 9 (2016) 653–662.
[58] S. Lebaschi, M. Hekmati, H. Veisi, Green synthesis of palladium nanoparticles mediated by black tea leaves (Camellia sinensis) extract: catalytic activity in the reduction of 4-nitrophenol and Suzuki-Miyaura coupling reaction under ligand-free conditions, J. Colloid Interface Sci. 485 (2017) 223–231.
[59] S. Banerjee, M.C. Chattopadhyaya, Adsorption characteristics for the removal of a toxic dye, tartrazine from aqueous solutions by a low cost agricultural by-product, Arab. J. Chem. 10 (2017) S1629–S1638.
[60] S. Naama, H. Menari, G. Nezzal, L. Baba, S. Lamrani, Enhancement of the tartrazine photodegradation by modi fi cation of silicon nanowires with metal nanoparticles, Mater. Res. Bull. 76 (2016) 317–326.
[61] G. Tekin, G. Ersoz, S. Atalay, Visible light assisted Fenton oxidation of tartrazine using metal doped bismuth oxyhalides as novel photocatalysts, J. Environ. Manage. 228 (2018) 441–450.
[62] C. Saravanan, R. Rajesh, T. Kaviarasan, K. Muthukumar, D. Kavitakea, P.H. Shettya, Synthesis of silver nanoparticles using bacterial exopolysaccharide and its application for degradation of azo-dyes, Biotechnol. Rep. 15 (2017) 33–40.
[63] K. Anand, K. Kaviyarasu, S. Muniyasamy, S.M. Roopan, R.M. Gengan, A.A. Chuturgoon, Bio-synthesis of silver nanoparticles using agroforestry residue and their catalytic degradation for sustainable waste management, J. Clust. Sci. 28 (2017) 2279–2291.
[64] M. Atarod, M. Nasrollahzadeh, S.M. Sajadi, Euphorbia heterophylla leaf extract mediated green synthesis of Ag/$TiO_2$ nanocomposite and investigation of its excellent catalytic activity for reduction of variety of dyes in water, J. Colloid Interface Sci. 462 (2016) 272–279.
[65] X. Liu, M. Liang, M. Liu, R. Su, M. Wang, W. Qi, Z. He, Highly efficient catalysis of azo dyes using recyclable silver nanoparticles immobilized on tannic acid-grafted eggshell membrane, Nanoscale Res. Lett. 11 (2016) 440.
[66] M. Nasrollahzadeh, M. Sajjadi, M. Maham, S.M. Sajadi, A.A. Barzinjy, Biosynthesis of the palladium/sodium borosilicate nanocomposite using Euphorbia milii extract and evaluation of its catalytic activity in the reduction of chromium (VI), nitro compounds and organic dyes, Mater. Res. Bull. 102 (2018) 24–35.
[67] A. Rostami-vartooni, M. Nasrollahzadeh, M. Alizadeh, Green synthesis of seashell supported silver nanoparticles using Bunium persicum seeds extract: application of the particles for catalytic reduction of organic dyes, J. Colloid Interface Sci. 470 (2016) 268–275.
[68] E. Alzahrani, Eco-friendly production of silver nanoparticles from peel of tangerine for degradation of dye, World J. Nano Sci. Eng. 5 (2015) 10–16.
[69] M.A. Behnajady, N. Modirshahla, R. Hamzavi, Kinetic study on photocatalytic degradation of C. I. Acid Yellow 23 by ZnO photocatalyst, J. Hazard. Mater. B 133 (2006) 226–232.
[70] S.K. Al-dawery, Photo-catalyst degradation of tartrazine compound in waste water using $TiO_2$ and UV light, J. Eng. Sci. Technol. 8 (2013) 683–691.
[71] A.A. Nada, H.R. Tantawy, M.A. Elsayed, M. Bechelany, M.E. Elmowafy, Elaboration of nano titania-magnetic reduced graphene oxide for degradation of tartrazine dye in aqueous solution, Solid State Sci. 78 (2018) 116–125.
[72] M. Darwish, A. Mohammadi, N. Assi, Microwave-assisted polyol synthesis and characterization of PVP-Capped CdS nanoparticles for the photocatalytic degradation of tartrazine, J. Mater. Res. Bull. 74 (2016) 387–396.
[73] K. Chanderia, S. Kumar, J. Sharma, R. Ameta, P.B. Punjabi, Degradation of Sunset Yellow FCF using copper loaded bentonite and $H_2O_2$ as photo-Fenton like reagent, Arab. J. Chem. 10 (2017) S205–S211.
[74] D. Rajamanickam, M. Shanthi, Photocatalytic mineralization of a water pollutant, Sunset Yellow dye by an advanced oxidation process using a modified catalyst, Toxicol. Environ. Chem. 95 (2013) 1484–1498.

[75] D. Rajamanickam, M. Shanthi, Photocatalytic degradation of an azo dye Sunset Yellow under UV-A light using $TiO_2$/CAC composite catalysts, Spectrochim, Acta Part A Mol. Biomol. Spectrosc. 128 (2014) 100–108.

[76] M. Rosu, M. Coros, F. Pogacean, L. Magerusan, C. Socaci, A. Turza, S. Pruneanu, Azo dyes degradation using $TiO_2$-Pt/GO and $TiO_2$-Pt/RGO photocatalysts under UV and natural sunlight irradiation, Solid State Sci. 70 (2017) 13–20.

[77] S. Zhang, Y. Liu, P. Gu, R. Ma, T. Wen, G. Zhao, L. Li, Y. Ai, C. Hu, X. Wang, Enhanced photodegradation of toxic organic pollutants using dual-oxygen-doped porous g-$C_3N_4$: Mechanism exploration from both experimental and DFT studies, Appl. Catal. B-Environ. 248 (2019) 1–10.

[78] A. Rostami-Vartooni, A. Moradi-Saadatmand, Green synthesis of magnetically recoverable $Fe_3O_4$/HZSM-5 and its Ag nanocomposite using Juglans regia L. leaf extract and their evaluation as catalysts for reduction of organic pollutants, IET Nanobiotechnol. 13 (2019) 407–415.

[79] B.R. Vergis, N. Kottam, R. Hari Krishna, B.M. Nagabhushana, Removal of Evans Blue dye from aqueous solution using magnetic spinel $ZnFe_2O_4$ nanomaterial: adsorption isotherms and kinetics, Nano-Struct. Nano-Objects 18 (2019) 100290.

[80] J. Mangalam, M. Kumar, M. Sharma, M. Joshi, High adsorptivity and visible light assisted photocatalytic activity of silver/reduced graphene oxide (Ag/rGO) nanocomposite for wastewater treatment, Nano-Struct. Nano-Objects 17 (2019) 58–66.